ASEG-PESA 2015
Geophysics and Geology together for Discovery
24th International Geophysical Conference and Exhibition
15–18 February 2015 Perth, Western Australia

Changes in elastic properties of artificial shales due to compaction

Roman Beloborodov
CSIRO Energy
Perth
BeloborodovRM@gmail.com

Marina Pervukhina
CSIRO Energy
Perth
Marina.Pervukhina@csiro.au

Lionel Esteban
CSIRO Energy
Perth
Lionel.Esteban@csiro.au

Maxim Lebedev
Curtin University
Perth
M.Lebedev@curtin.edu.au

SUMMARY

The effects of compaction on elastic properties of shales and their anisotropy are important for seismic imaging, seismic to well tie and borehole stability issues. Compaction trends in shales remain poorly studied, but it is well known that porosity of shales rapidly decreases with the increase of burial depth due to mechanical compaction and chemical transformation of clays in particular. These processes affect all the physical properties of shales including their elastic moduli, electrical conductivity and permeability.

In this experimental work we study changes in the anisotropic elastic properties of artificial shales caused by mechanical compaction. Investigation of anisotropy is performed on two specimens made of kaolinite and quartz powder mixtures: (1) 75% / 25 % and (2) 60% / 40%, respectively. An uniaxial stress is applied progressively to achieve distinct levels of porosity. Ultrasonic P- and S-wave velocities in the specimens are measured at every stage of the compaction. Thomsen's anisotropy parameters are calculated from these velocities. Qualitative characteristic of microfabric anisotropy is performed using micro-CT image analysis.

The results allow to conclude that at a given level of porosity of the specimen 2, with 40 % of quartz, has higher compressional and shear velocities than the specimen 1 with only 25% of quartz. However, the specimen 1 shows higher degree of elastic anisotropy than the specimen 2 due to higher fraction of anisotropic clay.

Key words: Compaction, anisotropy, elastic properties, porosity, artificial clay rocks, shales.

INTRODUCTION

Shale comprises about 70% of all sedimentary basins and understanding of shale lithogenesis is practically important for borehole stability and surface seismic interpretation. One of the main processes forming them is mechanical compaction and chemical mineral transformation (Hedberg, 1936; Rieke and Chilingarian, 1974). As a result the soft and highly porous sediment becomes an anisotropic solid rock with extremely low porosity and permeability.

Microfabric of shales is the most significant characteristic that defines their porosity, permeability, elastic moduli and mechanical strength. The microfabric of shales depends on a number of parameters such as clay and silt fraction, clay mineralogy, chemical composition of pore fluid, burial depth, etc. During compaction, clay particles may undergo re-orientation perpendicular to the maximum stress direction (Kawamura and Ogawab, 2004). Anisotropic shale microfabric explains the anisotropy of elastic, mechanical and fluid transport properties of these rocks.

During the last two decades lots of studies were dedicated to changes in properties and microfabric of clay rocks due to compaction (e.g., Vasseur et al., 1995; Djeran-Maigre et al., 1998; Aplin et al., 2006; Fawad et al., 2010; Moyano et al., 2012). The St. Austell kaolinite study, Vasseur et al. (1995) showed that the decrease in void ratio during compaction is caused specifically by particle re-orientation. Anisotropic orientation distribution function in shales also demonstrated to be responsible for anisotropy of the shale physical properties. Djeran-Maigre et al. (1998) showed that geomechanical properties of shales also depend on their mineralogical composition and mineral grain sizes.

In a series of experimental compaction tests, Fawad et al. (2010) observed that orientation of clay particles in clay-silt mixtures depends on the maximum confining stress and the silt fraction content. A silt grain supported framework dictates the orientation of the clay particles at large confining stresses. In silt-clay mixtures, in which the clay matrix is load bearing, the alignment of clay particles increases with the increase of clay content, the size of the clay particles and the stress. Velocities in a silt-clay mixture depend not only on its porosity but also on its microstructure.

Properties of clay-bearing rocks and their evolution with the increase of burial depth were studied by Dewhurst et al. (1998), Mondol et al. (2007), Voltolini et al. (2009), Moyano et al. (2012). Mondol et al. (2008) and Voltolini et al. (2009) investigated dependency between the burial depth (a proxy of the experienced stress) and physical properties of shales such as porosity, permeability and ultrasonic velocities. Mondol et al. (2007) found that compressibility of mudstones mainly depend on the type and content of clay minerals, amount of pore fluids and pore pressure. These experimental studies confirm complicated relations between the burial depth and physical properties of shales. Pure argillaceous sediments also exhibit very broad correlation between the burial depth and their physical properties.

A study of compaction trend in mudstones (Dewhurst et al., 1998) showed that porosity-permeability relationships were strongly influenced by the lithology and the grain size distribution. Although the porosity of the silt-rich clay rocks is

lower than that of the clay-rich ones, its permeability is from 40 to 200 times greater at a given level of porosity.

Most of the above works were fulfilled on natural shale and mudstone samples. With such material, an accurate control of compaction environment including clay mineralogy, temperature, clay and silt particle sizes and pore fluid chemistry is hardly possible. At the same time, a study of transformation of the silt-clay mixtures into shales under controlled conditions with simultaneous recording of the shale microfabric, porosity and ultrasonic velocities could give a new insight on the nature of physical anisotropy in shales. Here we compact two samples made of kaolinite and quartz powder mixtures. The kaolinite to quartz ratios are 3:1 and 3:2 in the first and the second sample, respectively. Uniaxial stress is progressively applied to achieve different levels of porosity. Ultrasonic P- and S-wave velocities in the specimens are measured at every step during experiments. Thomsen's anisotropy parameters are calculated from these velocities. Qualitative characteristic of microfabric anisotropy is also performed using micro-CT image analysis before and after compaction.

MATERIALS AND METHODS

Specimen preparation

Two specimens are prepared for compaction with a kaolinite and quartz mixture as 75% - 25% (specimen 1) and 60 % - 40% (specimen 2), respectively. The silt fraction consists of quartz grains with size up to 100 µm in diameter. The clay fraction consists of pure kaolinite with grain sizes < 1 µm. Dry densities of quartz and kaolinite powders are obtained with helium gas displacement pycnometry method at 2.65 and 2.61, respectively.

The quartz and kaolinite powders are dried at 105°C during six hours to assure their constant masses. Then, the dry powders are mixed together to obtain a homogeneous mixture and diluted with 75 g/l KCl brine solution with a pH of 7.32.

Compaction

Compaction of slurries is performed in a high-pressure oedometer cell. It allows to apply an uniaxial stress up to 150 MPa. Liquids and gases could easily pass through the porous pistons at the top and bottom of the cell. Uniaxial stress is progressively applied by increasing steps to achieve the required porosity value. We assume that each specimen is fully saturated with water and completely fills the volume of the cell. Porosity of the specimen is estimated as function of change of its volume using the following relationship:

$$\phi = \frac{V_0 - (m_q/\rho_q + m_k/\rho_k)}{V_0}, \quad (1)$$

where ϕ is the porosity, V_0 (in cm^3) is the initial sample bulk volume computed from the initial specimen height and the oedometer cross-section area, m_q and m_k are the mass (in g) of the dry quartz and kaolinite, and ρ_q and ρ_k are the specific densities of quartz and kaolinite grains (in g/cm^3).

Velocity measurements

The oedometer is equipped with two sets of piezoelectric transducers, which allow measuring ultrasonic P- and S-wave velocities along and normal to the applied stress direction. The pulse transmission technique (Birch, 1960) is used to measure compressional and shear wave velocities. At every applied pressure step, transit times of the ultrasonic waves are measured with an oscilloscope on both orthogonal directions. Velocities are calculated using the following equation:

$$V = L/(t - t_0), \quad (2)$$

where V (in m/s) is either P- or S-wave velocity, L is the sample length (in m), t is the travel time (in s) along the sample length and t_0 is the delay time (in s) between the transducers.

When the specimen reached the targeted minimal porosity, it is gently ejected from the oedometer cell and placed into oil to preserve it from major desiccation. The velocities of each sample at each desired compaction/porosity stage are measured in three orthogonal directions and at 45 degrees from the vertical axis.

RESULTS

Values of density and porosity of specimens before and after compaction are presented in Table 1.

Table 1. Physical parameters of specimens at the beginning (ρ_0, ϕ_0) and the end (ρ, ϕ) of compaction tests.

		Specimen 1	Specimen 2
Quartz-kaolinite ratio		25/75	40/60
ρ_0	(g/cm^3)	1.52	1.50
ρ	(g/cm^3)	2.21	2.23
ϕ_0	(%)	68	69
ϕ	(%)	25	24

During the compaction, anisotropy of the specimens may be estimated only by simple ratio of velocities of compressive P-waves in orthogonal directions (Figure 1). It is important to note that in this case only so-called P-wave anisotropy or Thomsen's anisotropy parameter ε could be obtained. Before the compaction process, the high quartz content specimen 2 shows higher degree of anisotropy than specimen 1. During compaction, anisotropy of specimens degrades until to become negligible when specimens 1 and 2 reach 65% and 54% of porosity, respectively. Further compaction leads to growth of anisotropy in both specimens, with a higher degree of anisotropy for the specimen 2.

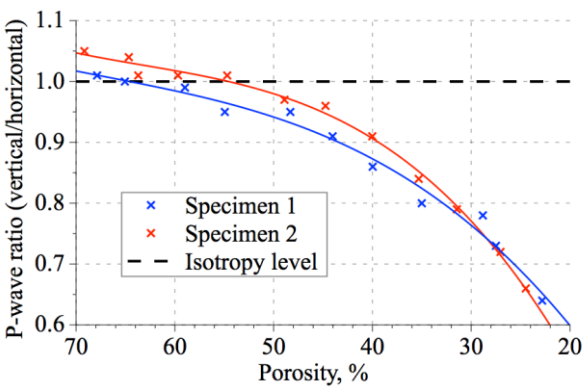

Figure 1. Vertical to horizontal P-wave velocities ratios vs porosity.

Compressional P-wave and shear S-wave velocities as a function of porosity (Figure 2) shows similar trends for the two investigated specimens.

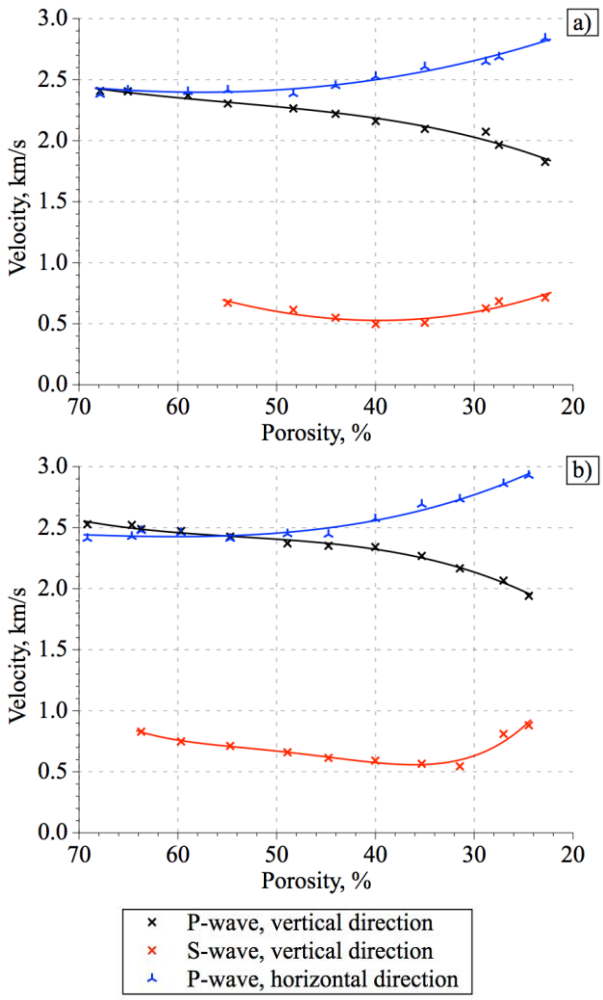

Figure 2. P- and S-waves velocities vs porosity: (a) in specimen 1 with 3:1 kaolinite to quartz ratio, (b) in specimen 2 with 3:2 kaolinite to quartz ratio.

The porosity reduction induces the gradual decrease of the P-wave velocity along the stress axis (i.e. normal to bedding) from 2.4 to 1.8 km/s for specimen 1 and simultaneously an increase of the P-wave velocity transversally to the stress direction (i.e. parallel to the bedding plane) from 2.4 to 2.8 km/s. Velocities in specimen 2 are about 100 m/s higher than in specimen 1 independently of the porosity. This might be explained with higher quartz content in specimen 2, which has higher elastic moduli than kaolinite. During compaction, shear wave velocity along the stress direction for specimens 1 and 2 decreases slightly from 0.7 km/s and 0.8 km/s, repectively, and reaches a minimum of about 0.5 km/s and 0.6 km/s at ~ 40% and 30% of porosity, respectively. Toward lower porosity decrease, shear wave velocity rapidly grows back to 0.8 and 0.9 km/s in specimens 1 and 2.

Elastic constants

Elastic constants and Thomsen's anisotropy parameters are shown in Tables 2 and 3 for both investigated samples at a porosity of about 24%.

Table 2. Elastic constants - five components of the stiffness tensor for a transversely isotropic material

		Specimen 1	Specimen 2
Quartz-kaolinite ratio		25/75	40/60
C_{11}	(GPa)	8.02	8.29
C_{33}	(GPa)	5.23	6.20
C_{13}	(GPa)	—	4.62
C_{44}	(GPa)	0.79	0.87
C_{66}	(GPa)	1.18	0.94

Table 3. Thomsen's parameters for transversely isotropic elastic material, where P- and S-waves denoted by α, β, respectively, and ε, γ, δ characterize anisotropy.

		Specimen 1	Specimen 2
Quartz-kaolinite ratio		25/75	40/60
α	(km/s)	1.54	1.66
β	(km/s)	0.60	0.62
ε		0.27	0.17
γ		0.25	0.04
δ		—	0.03

Micro-CT tomogram images are obtained with an XRadia VersaXRM-500 tomograph with a spatial voxel resolution of 0.9x0.9x0.9 μm^3. Analysis of micro-CT images is performed with "Image-J 2" software to reconstruct 3D spatial orientations of quartz particles. A stack of 100 images normal to bedding is chosen for statistical analysis of quartz grain orientation. The quartz grains are first segmented from each image (Figure 3b) and their shapes are approximated within ellipses (Figure 3c). The angle between the long axis of each ellipse and the horizontal axis is calculated to plot the rose diagrams of quartz particles orientation (Figure 4c).

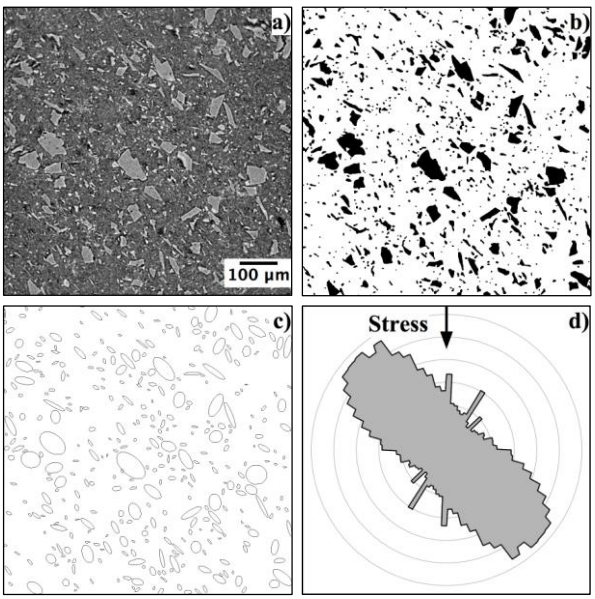

Figure 3. Micro-CT Image-J analysis of compaction effect on quartz-kaolinite mixture from specimen 1 (cross-section normal to the bedding plane). (a) raw image; (b) segmentation of quartz grains; (c) ellipse fitting each quartz grain and (d) rose-chart showing the orientation of the long axis of ellipse fitting the quartz grain.

Analysis of micro-CT images shows that, at similar porosity (about 25%), most of the quartz grains in specimen 1 are oriented at 45º (Figure 3d) from the applied pressure direction, whereas in specimen 2 the quartz grains are oriented almost

perpendicular to it (Figure 4d). We suggest that a load bearing skeleton is formed on the quartz grains (silt size) in the specimen 2 rich in quartz. This hypothesis is indirectly confirmed with the higher ultrasonic velocity measurements in specimen 2 than in specimen 1 in which kaolinite (clay size) is load bearing. More detailed 3D analysis should be investigated to understand the connectivity of both quartz and kaolinite phases in the samples; and evaluate with further experiments the grain size effect (similar mineralogy) versus the mineral effect (similar particle sizes).

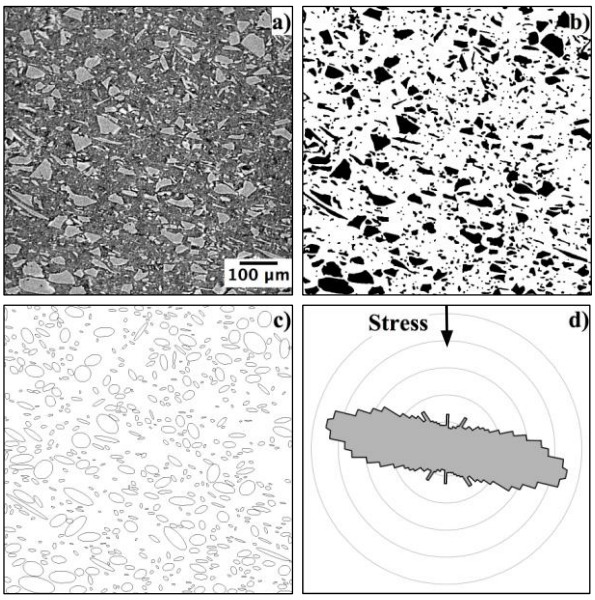

Figure 4. Micro-CT Image-J analysis of compaction effect on quartz-kaolinite mixture from specimen 2 (cross-section normal to the bedding plane). (a) raw image; (b) segmentation of quartz grains; (c) ellipse fitting each quartz grain and (d) rose-chart showing the orientation of the long axis of ellipse fitting the quartz grain.

CONCLUSIONS

Current study has shown that compaction of clayey suspensions leads to drastic changes in their microfabric and anisotropy of physical and elastic parameters. The increase of the quartz fraction (silt size) has resulted in the increase of elastic waves velocities and has caused stronger alignment of kaolinite clay fraction (clay size) in compacted artifical shales. At the same time, the sample with the lowest quartz content exhibited higher Thomsen's anisotropy parameters what could be explained with the strong anisotropy of kaolinite compared to quartz, though grain size effect must be investigated independently to fully conclude. These preliminary results are in a good agreement with the previous studies and could be used for prediction of elastic properties and anisotropy of natural shales.

ACKNOWLEDGMENTS

Authors would like to acknowledge Dr. Matthew Josh for sharing the quartz and kaolinite powders. Roman Beloborodov thanks CSIRO Capability Development Fund that supported this study. The authors thank the National Geosequestration Laboratory (NGL) for providing access to the X-ray microscope VersaXRM-500 (Xradia Ltd). The NGL is a collaboration between CSIRO, the University of Western Australia and Curtin University established to conduct and deploy critical research and development to enable commercial-scale carbon storage options. Funding for this facility was provided by the Australian Federal Government.

REFERENCES

Aplin, A.C., Matenaar, I.F., McCarty, D.K., Van der Pluijm, B.A., 2006. Influence of mechanical compaction and clay mineral diagenesis on the microfabric and pore-scale properties of deep-water Gulf of Mexico mudstones. Clays and Clay Minerals 54, 500–514.

Birch, A.F., 1960. The velocity of compressional waves in rocks to 10 kilobars; Part 1. Journal of Geophysical Research 65 (4), 1083–1102.

Dewhurst, D.N., Aplin, A.C., Sarda, J.P., Yang, Y.L., 1998. Compaction-driven evolution of porosity and permeability in natural mudstones: an experimental study. J. Geophys. Res. 103, 651–661.

Djeran-Maigre, I., Tessier, D., Grunberger, D., Velde, B., Vasseur, G., 1998. Evolution of microstructures and of macroscopic properties of some clays during experimental compaction. Marine and Petroleum Geology 15, 109–128.

Fawad, M., Mondol, N.H., Jahren, J., Bjorlykke, K., 2010. Microfabric and rock properties of experimentally compressed silt-clay mixtures. Marine and Petroleum Geology 27, 1698-1712.

Hedberg, H. D., 1936. Gravitational compaction of clays and shales Am, J. Sci. 231,241-278.

Kawamura, K., and Y. Ogawab, 2004, Progressive change of pelagic clay microstructure during burial process: Examples from piston cores and ODP cores: Marine Geology, 207, 131–144.

Mondol, N. H., K. Bjorlykke, J. Jahren, and K. Hoeg, 2007, Experimental mechanical compaction of clay mineral aggregates — Changes in physical properties of mudstones during burial: Marine and Petroleum Geology, 24, 289–311.

Mondol, N. H., K. Bjorlykke, and J. Jahren, 2008, Experimental compaction of clays: Relationship between permeability and petrophysical properties in mudstones: Petroleum Geoscience, 14, 319–337.

Moyano, B., Spikes, K.T., Johansen, T.A. & Mondol, N.H., 2012. Modeling compaction effects on the elastic properties of clay-water composites, Geophysics, 77, D171–D183.

Rieke, III. H. H. and Chilingarian, G. V. (1974) Compaction of Argillaceous Sediments Dev. Sedimentol. No. 16, Elsevier, Amsterdam, 424 pp

Vasseur, G., Djeran-Maigre, I., Grunberger, D., Rousset, G., Tessier, D., Velde, B., 1995. Evolution of structural and physical parameters of clays during experimental compaction. Marine and Petroleum Geology 12, 941–954.

Voltolini, M., Wenk, H.R., Mondol, N.H., Bjørlykke, K., Jahren, J., 2009. Anisotropy of experimentally compressed kaolinite–illite–quartz mixtures. Geophysics 74, D13–D23.